Title

GLP-1 Cleavage Product Reverses Persistent ROS Generation After Transient Hyperglycemia by Disrupting an ROS-Generating Feedback Loop.

Journal

Diabetes, 64(9)

ISSN

0012-1797

Authors

Giacco, Ferdinando
Du, Xueliang
Carratú, Anna
et al.

Publication Date

2015-09-01

DOI

10.2337/db15-0084

Peer reviewed

Ferdinando Giacco,[1,2] Xueliang Du,[1,2] Anna Carratú,[3] Gary J. Gerfen,[4] Maria D'Apolito,[5] Ida Giardino,[6] Andrea Rasola,[7] Oriano Marin,[7] Ajit S. Divakaruni,[8] Anne N. Murphy,[8] Manasi S. Shah,[1,2] and Michael Brownlee[1,2,9]

GLP-1 Cleavage Product Reverses Persistent ROS Generation After Transient Hyperglycemia by Disrupting an ROS-Generating Feedback Loop

Diabetes 2015;64:3273–3284 | DOI: 10.2337/db15-0084

The assumption underlying current diabetes treatment is that lowering the level of time-averaged glucose concentrations, measured as HbA_{1c}, prevents microvascular complications. However, 89% of variation in risk of retinopathy, microalbuminuria, or albuminuria is due to elements of glycemia not captured by mean HbA_{1c} values. We show that transient exposure to high glucose activates a multicomponent feedback loop that causes a stable left shift of the glucose concentration-reactive oxygen species (ROS) dose-response curve. Feedback loop disruption by the GLP-1 cleavage product GLP-1(9–36)^{amide} reverses the persistent left shift, thereby normalizing persistent overproduction of ROS and its pathophysiologic consequences. These data suggest that hyperglycemic spikes high enough to activate persistent ROS production during subsequent periods of normal glycemia but too brief to affect the HbA_{1c} value are a major determinant of the 89% of diabetes complications risk not captured by HbA_{1c}. The phenomenon and mechanism described in this study provide a basis for the development of both new biomarkers to complement HbA_{1c} and novel therapeutic agents, including GLP-1(9–36)^{amide}, for the prevention and treatment of diabetes complications.

The assumption underlying current clinical treatment of type 1 diabetes is that lowering the level of time-averaged glucose concentrations, measured as HbA_{1c}, prevents the development and progression of vascular complications. This current treatment recommendation, adopted by diabetes professional societies around the world, is based on data from the Diabetes Control and Complications Trial (DCCT) (1), where the intensive treatment group had a 73% reduction in risk of sustained retinopathy progression compared with the standard treatment group.

Of note, subsequent analysis of DCCT data by the DCCT/Epidemiology of Diabetes Interventions and Complications (EDIC) Research Group showed that for the entire study population, HbA_{1c} values explained only 6.6–11% of the risk of retinopathy, albuminuria, or microalbuminuria. The DCCT/EDIC Research Group concluded that the unexplained 89% of variation in risk is due to elements of glycemia not captured by mean HbA_{1c} values (2,3). The nature and identity of those elements are not yet understood.

HbA_{1c} represents the time-averaged mean level of glycemia and thus provides no information about how closely the fluctuations of blood glucose levels around that mean mimic the normal narrow range of blood glucose excursion. Continuous glucose monitoring data show that in patients with type 1 diabetes with identical HbA_{1c} values, amplitude and duration of glycemic spikes differ significantly (4). This suggests to us that a potential major determinant of complications not captured by HbA_{1c}

[1]Diabetes Research Center, Albert Einstein College of Medicine, Bronx, NY
[2]Department of Medicine, Albert Einstein College of Medicine, Bronx, NY
[3]Department of Pharmaceutical and Biomedical Sciences, University of Salerno, Salerno, Italy
[4]Department of Physiology and Biophysics, Albert Einstein College of Medicine, Bronx, NY
[5]Institute of Pediatrics, Department of Medical and Surgical Sciences, University of Foggia, Foggia, Italy
[6]Department of Clinical and Experimental Medicine, University of Foggia, Foggia, Italy
[7]Department of Biomedical Science, University of Padua, Padua, Italy
[8]Department of Pharmacology, University of California, San Diego, La Jolla, CA
[9]Department of Pathology, Albert Einstein College of Medicine, Bronx, NY
Corresponding author: Michael Brownlee, michael.brownlee@einstein.yu.edu.

Received 20 January 2015 and accepted 6 May 2015.
This article contains Supplementary Data online at http://diabetes.diabetesjournals.org/lookup/suppl/doi:10.2337/db15-0084/-/DC1.
F.G. and X.D. contributed equally to this work.

could be hyperglycemic spikes high enough to activate complication-causing mechanisms but too brief to affect the HbA_{1c} value (5).

Because hyperglycemia-induced overproduction of mitochondrial reactive oxygen species (ROS) initiates many of the complex series of molecular events that result in diabetic tissue damage (6), we hypothesized that transient exposure to high glucose causes persistent mitochondrial overproduction of ROS during subsequent prolonged periods of normal glucose. Mitochondrial ROS generation increases when the inner mitochondrial transmembrane potential ($\Delta\Psi$) exceeds a threshold level (7). Maintaining a constant level of $\Delta\Psi$ requires binding of the glycolytic enzyme hexokinase II (HK-II) to the outer mitochondrial membrane protein VDAC (voltage-dependent anion channel). The HK-II/VDAC association is regulated by several mechanisms (8–10). Because activated glycogen synthase kinase-3β (GSK-3β) phosphorylates VDAC in the mitochondrial outer membrane of HeLa cells, preventing VDAC association with hexokinase (11), we speculated that in vascular cells, activation of GSK-3β by transient hyperglycemia could be a critical element in a multicomponent feedback loop that would maintain persistently increased ROS production during subsequent periods of normoglycemia.

GLP-1(9–36)^{amide}, originally considered to be an inactive degradation product of GLP-1(7–36)^{amide}, has important physiologic effects distinct from GLP-1 (12). In hippocampal slices from the APP/presenilin 1 (PS1) mouse model of Alzheimer disease, continuous exposure to this GLP-1 cleavage product reduced elevated mitochondrial superoxide and increased levels of the inhibitory phosphorylation of GSK-3β at serine 9 (13).

In the current study, we show that transient exposure to high glucose activates a multicomponent feedback loop involving mitochondrial superoxide-induced release of free iron and H_2O_2. As a consequence, protein phosphatase 2 (PP2A) is activated and dephosphorylates Akt1, reducing its activity. Reduced Akt1 activity decreases inhibitory phosphorylation of GSK-3β, resulting in increased phosphorylation of VDAC. Impaired association of phosphorylated VDAC with the glycolytic enzyme hexokinase causes a stable left shift of the glucose concentration-ROS dose-response curve (Fig. 3). Feedback loop disruption by the GLP-1 cleavage product GLP-1(9–36)^{amide} reverses the persistent left shift, thereby normalizing persistent ROS production and its pathophysiologic consequences in cultured endothelial cells and in mice after transient hyperglycemia.

RESEARCH DESIGN AND METHODS

Cell Culture Conditions and Materials

Human aortic endothelial cells (HAECs) were from Invitrogen (Grand Island, NY) and maintained in endothelial cell growth medium-2 containing 0.4% FBS plus growth factor additives obtained from Lonza (Walkersville, MD). Microcystin, okadaic acid, and deferoxamine mesylate used at 25 nmol/L, 0.1 μg/mL, and 100 μmol/L, respectively, were from Sigma-Aldrich (St. Louis, MO). [γ^{32}P]ATP was from GE Healthcare Life Sciences (Piscataway, NJ). TAT-Scr and TAT-HK peptides used at 10 μmol/L were synthesized as previously described (14). To prevent TAT-HK–induced cell death (14), cells treated with TAT-HK and TAT-Scr were pretreated for 1 h with 1 μmol/L cyclosporin A. GLP-1(9–36)^{amide} used at 100 pmol/L was from Bachem (Torrance, CA). GSK-3β inhibitory peptide used at 10 μmol/L was obtained from EMD (San Diego, CA). Antibodies to GSK-3β, p-GSK-3β (S9), HK-II, and VDAC were from Cell Signaling Technology (Danvers, MA), BD Bioscience (San Diego, CA), and Santa Cruz Biotechnology (Dallas, TX), respectively. Antibodies to p-Thr were from Invitrogen. Mitochondrial isoform of superoxide dismutase (Mn-SOD), empty vector, and catalase adenovirus were obtained as previously described (15). Constitutively active GSK-3β adenovirus and plasmids containing constitutively activated Akt1 (Akt-1CA) and dominant negative Akt (Akt-DN) were gifts from M. Birnbaum, University of Pennsylvania. Akt-1CA and Akt-DN cDNAs were subcloned into a shuttle vector for adenoviral particle packaging (15). Adenoviruses were used at a multiplicity of infection of 100. Six- to 8-week-old C57BL/6 mice were purchased from The Jackson Laboratory (Bar Harbor, ME).

ROS Measurement

Cells were plated in 96-well cell culture plates. Intracellular ROS were detected using the fluorescent probe CM-H_2DCFDA, which reacts with superoxide, H_2O_2, hydroxyl radical, and $ONOO^-$. Cells were loaded with 10 μmol/L CM-H_2DCFDA after two washes with no phenol red minimum essential medium, incubated for 45 min at 37°C, and analyzed with an HTS 7000 Bio Assay Fluorescent Plate Reader (PerkinElmer) using the HTSoft program (16).

Mitochondrial Membrane Potential Measurement

Mitochondrial membrane potential was assessed using JC-1 dye from Life Technologies.

Immunoprecipitation and Western Blotting

Immunoprecipitation (IP) and Western blot (WB) experiments were performed as previously described (15).

Determination of Kinase Activity

GSK-3β and Akt1 activities were measured using a kit from Sigma-Aldrich and Cell Signaling Technology, respectively. The effect of GLP-1(9–36)^{amide} on Akt1 activity was measured as described in the Supplementary Data.

Determination of PP2A Activity

PP2A activity was analyzed using a kit from R&D Systems.

Determination of Intracellular Free Iron

Free iron was measured by electron paramagnetic resonance (EPR) using a modification of the method described by Srinivasan et al. (17). See Supplementary Data for details.

Induction of Transient Hyperglycemia in Nondiabetic, Normoglycemic Mice

Transient hyperglycemia was induced as previously described (18).

Prostacyclin Synthase Activity

Prostacyclin synthase (PGI_2) activity was measured by determination of 6-keto-PGF-1α as previously described (19).

Statistics

ROS data are expressed as mean ± SEM. All other data are expressed as mean ± SD. ANOVA in conjunction with the Tukey-Kramer test was used for comparison of experimental groups. Statistical analyses were performed using PHStat2 software.

RESULTS

Transient Exposure to High Glucose Induces Persistent Mitochondrial ROS Production by Shifting the Glucose Concentration-ROS Curve to the Left

Exposure of HAECs to 25 mmol/L glucose for 6 h induced a 2.5-fold increase in ROS production (Fig. 1*A*, bar 2). Of note, the increase in ROS production induced by 6 h of 25 mmol/L glucose persisted for 2 days of subsequent incubation in 5 mmol/L glucose (Fig. 1*A*, bar 3). The increased ROS production induced by transient high glucose was prevented by overexpression of Mn-SOD (Fig. 1*A*, bar 4). Mn-SOD overexpression was confirmed by Western blot (data available on request). Cu/Zn-SOD also prevented a high glucose–induced increased ROS (Supplementary Fig. 1). The observations that both Mn-SOD and Cu/Zn-SOD prevent glucose-induced ROS are best explained by a mitochondrial origin of superoxide with Cu/Zn-SOD carrying out dismutation in the mitochondrial intermembrane space. To determine the exposure time necessary to reach the ROS levels observed at 6 h, a time course experiment was performed in which HAECs were exposed to 25 mmol/L glucose for increasing times up to 6 h (Fig. 1*B*). Maximal ROS levels were reached at 1 h and unchanged after 2–6 h exposure to high glucose (Fig. 1*B*). Because maximal ROS levels were reached after 1 h of exposure to 25 mmol/L glucose, a similar time-course experiment was performed to determine how many hours of transient high glucose were required to induce persistent elevation of ROS production after 2 days' exposure to 5 mmol/L glucose (Fig. 1*C*). Although only 1 h of exposure to 25 mmol/L glucose was sufficient to induce maximal ROS production (Fig. 1*B*), induction of persistent elevation of ROS production for 2 days of subsequent exposure to 5 mmol/L glucose required a minimum of 4 h transient exposure to 25 mmol/L glucose (Fig. 1*C*).

To understand how 6 h of exposure to 25 mmol/L glucose caused persistent elevation of ROS production during 2 days of subsequent exposure to 5 mmol/L glucose, cells were incubated for 6 h in either 5 or 25 mmol/L glucose. Both groups of cells were then incubated in 5 mmol/L glucose for 2 days. After that 2-day incubation in 5 mmol/L glucose, cells from both groups were exposed to various concentrations of glucose for 6 h and ROS measured using CM-H_2DCFDA (Fig. 1*D*).

In the dose-response curve from cells exposed only to 5 mmol/L glucose, ROS production did not increase significantly between glucose concentrations of 5 and 8 mmol/L. From 9 to 12 mmol/L glucose, ROS production increased rapidly until reaching a maximum at 12 mmol/L. Further increases in ROS were not induced by exposure to higher concentrations of glucose. In contrast, cells transiently preexposed to 25 mmol/L glucose showed a left shift in the glucose concentration-ROS dose-response curves after 2 days' exposure to 5 mmol/L glucose. In these cells, ROS production increased rapidly from 2.5 to 5 mmol/L glucose, reaching the same maximal level at 5 mmol/L glucose as the maximal level reached at 12 mmol/L in cells incubated only in 5 mmol/L glucose. Further increases in ROS were not induced by exposure to concentrations of glucose >5 mmol/L.

Persistent Mitochondrial ROS Production After Transient Exposure to High Glucose Is Maintained by a Multicomponent Feedback Loop

Transient Exposure to High Glucose Induces a Persistent Reduction in HK-II/VDAC Association

Mitochondrial ROS generation increases when $\Delta\Psi$ exceeds a threshold level (7). Maintaining a constant level of $\Delta\Psi$ requires binding of the glycolytic enzyme HK-II to the outer mitochondrial membrane protein VDAC. This binding regulates shuttling of ATP out of and ADP into the mitochondrial matrix.

In HAECs, $\Delta\Psi$ and ROS were both increased by 6 h of exposure to 25 mmol/L glucose (Fig. 2*A*, top and bottom panels). In 5 mmol/L glucose, dissociation of HK-II from VDAC induced by a cell-permeable HK-II N-terminal peptide, HK-TAT (14), caused an increase in HAEC $\Delta\Psi$ and ROS identical to that induced by exposure to 25 mmol/L glucose for 6 h (Fig. 2*A*, top and bottom panels). Moreover, maximal respiration was reduced by ~38% after 6 h of exposure to 25 mmol/L glucose (Supplementary Fig. 2). This result suggests that oxidative damage to enzymes of the tricarboxylic acid cycle, the electron transport chain (ETC), or the inner mitochondrial membrane lipids occurred by 6 h of 25 mmol/L glucose incubation (20,21).

Because dissociation of HK-II from VDAC in the presence of 5 mmol/L glucose increased HAEC $\Delta\Psi$ and ROS production to the same extent as exposure of these cells to 25 mmol/L glucose, we next asked whether exposure of HAECs to 25 mmol/L glucose would cause dissociation of HK-II from VDAC. The association of HK-II with VDAC was evaluated by coimmunoprecipitation (IP:VDAC, WB:HK-II) after 1, 2, 3, 4, 5, and 6 h of exposure of HAECs to 25 mmol/L glucose (Fig. 2*B*). HK-II/VDAC association was reduced by 50% at 3 h and by 75% at 6 h. Consistent with the persistence of increased ROS production in 5 mmol/L glucose after transient exposure to 25 mmol/L glucose, the HK-II dissociation from VDAC induced by 6 h of exposure to 25 mmol/L glucose also persisted for 2 days of subsequent exposure to 5 mmol/L glucose (Fig. 2*B*, red bar).

HK-II/VDAC association is regulated by several mechanisms (8–10). VDAC threonine phosphorylation by GSK-3β causes detachment of HK-II from VDAC (8). To determine whether the HK-II/VDAC dissociation induced by transient exposure to high glucose was caused by increased threonine VDAC phosphorylation, IP-WB experiments were performed

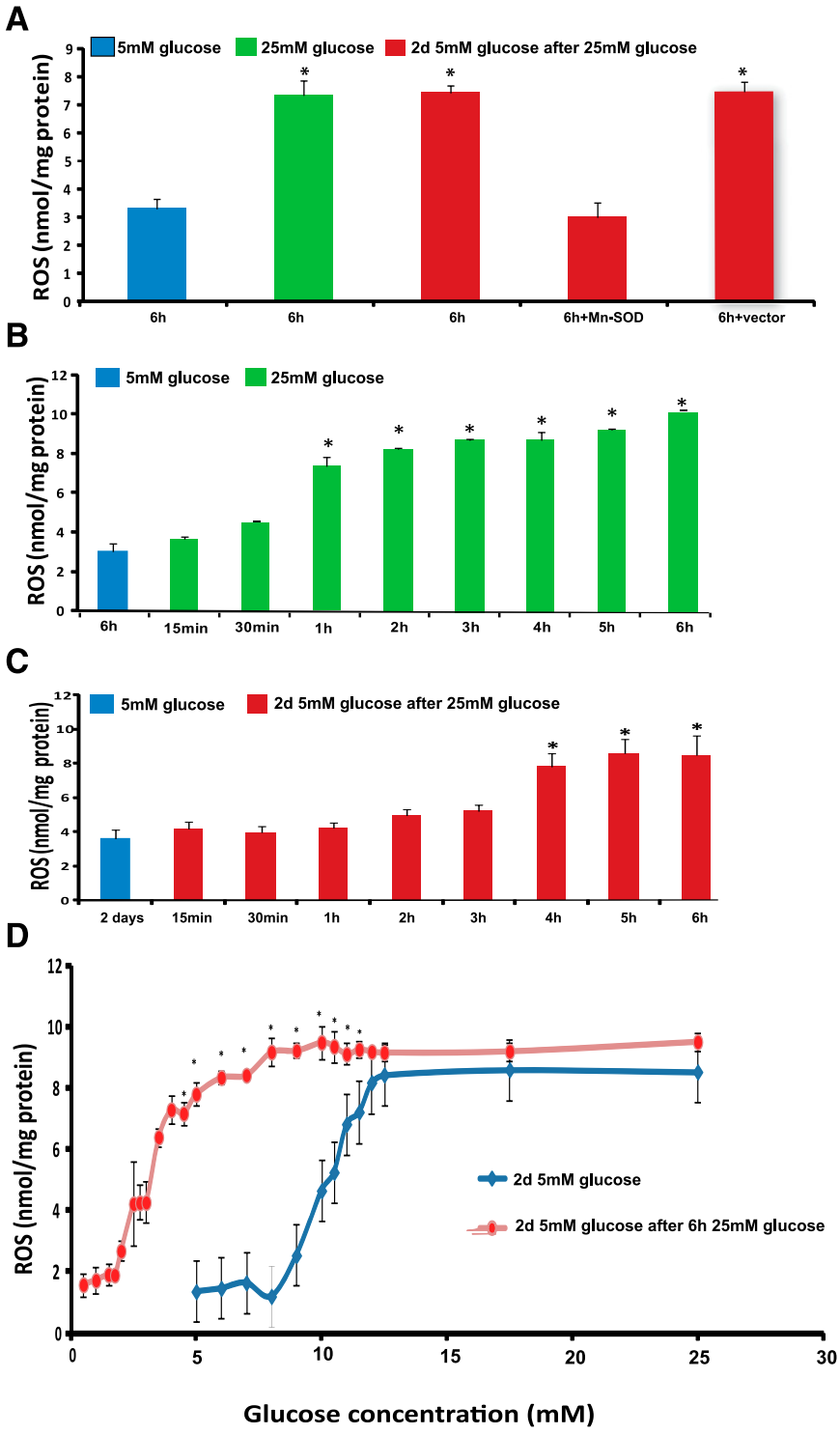

Figure 1— Transient exposure to high glucose induces persistent mitochondrial ROS production by shifting the glucose concentration-ROS curve to the left. *A*: ROS levels in HAECs exposed to 25 mmol/L glucose for 6 h (green bar) and 25 mmol/L glucose for 6 h followed by 2 days (d) of subsequent incubation in 5 mmol/L glucose (red bars). In the indicated groups, cells were infected with Mn-SOD or control adenoviral vectors before transient exposure to 25 mmol/L glucose. *B*: ROS levels in HAECs exposed to 25 mmol/L glucose for varying times. *C*: ROS levels after 2 days of incubation in 5 mmol/L glucose following transient exposure to 25 mmol/L glucose for varying times. *D*: Glucose concentration-ROS dose-response curves from HAECs transiently exposed to 25 mmol/L glucose (6 h) and then to 5 mmol/L glucose for 2 days (red line) and from HAECs exposed to 5 mmol/L glucose for 6 h continued for 2 days (blue line). ROS levels were measured by CM-H_2DCFDA. Data are mean ± SEM from three independent experiments with at least eight technical replicates. *$P < 0.05$.

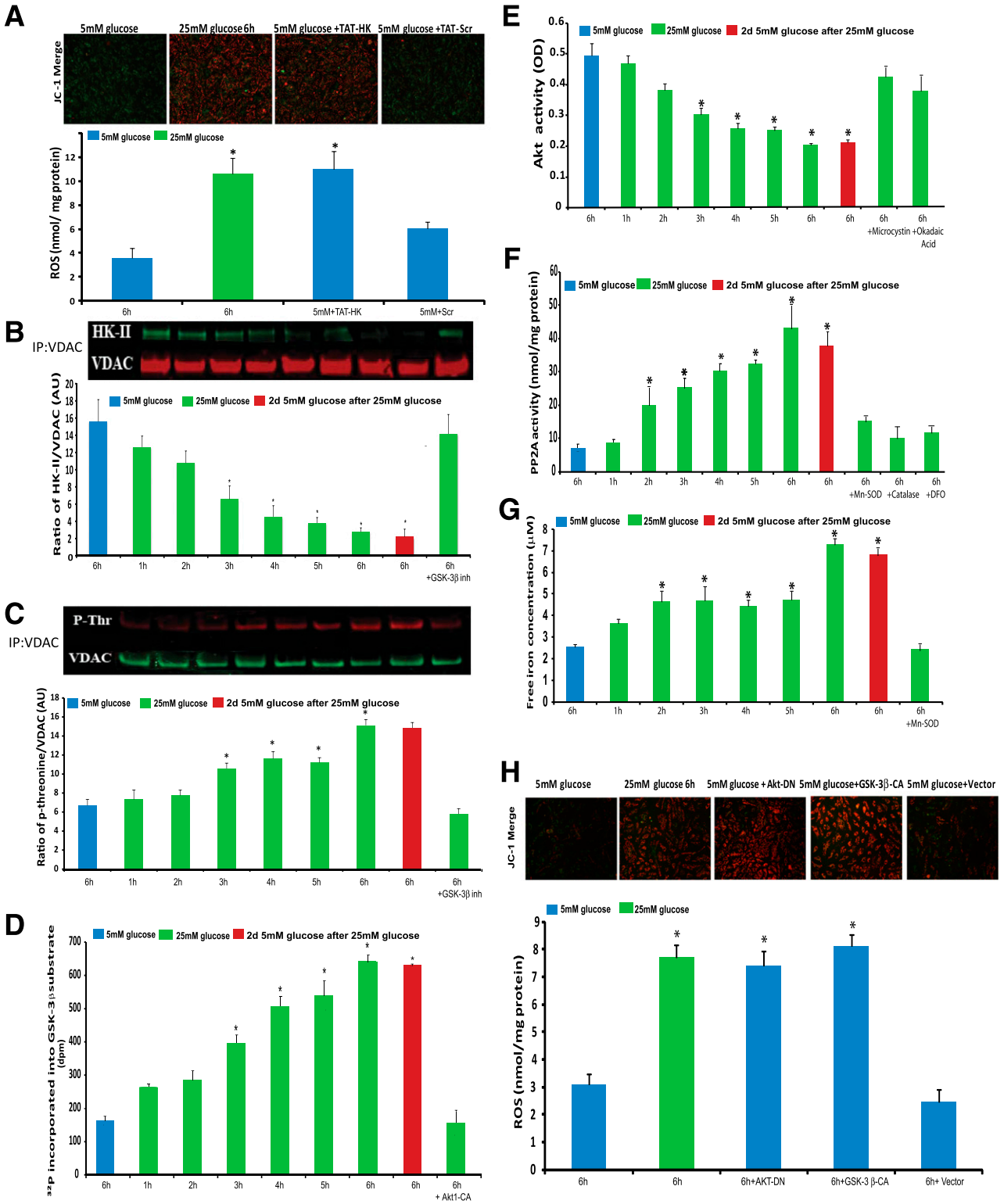

Figure 2—Persistent mitochondrial ROS production after transient exposure to high glucose is maintained by activation of a multicomponent feedback loop. *A*: Inner mitochondrial transmembrane potential and ROS level in HAECs after transient exposure to 25 mmol/L glucose or dissociation of HK-II from VDAC with the cell-permeable HK-II N-terminal peptide HK-TAT in 5 mmol/L glucose. Top panel shows representative photomicrographs of increased JC-1 red fluorescence, indicating increased mitochondrial membrane potential. Bottom panel shows ROS production measured by CM-H_2DCFDA. *B–G*: HAECs were exposed to 25 mmol/L glucose for the indicated times with (red bars) or without (green bars) subsequent incubation in 5 mmol/L glucose for 2 days (d). Cells exposed to 5 mmol/L glucose were used as controls (blue bars). *B*: HK-II/VDAC association after transient exposure of HAECs to high glucose, after 2 days of 5 mmol/L glucose following 6 h of 25 mmol/L glucose, and after 6 h of exposure to 25 mmol/L in the presence of a peptide inhibitor of GSK-3β. Top panel shows IP-WB of VDAC:VDAC and VDAC:HK-II. Bottom panel shows quantitation of IP-WB data from top panel. *C*: VDAC phosphorylation after transient exposure of HAECs to high glucose, after 2 days of 5 mmol/L glucose following 6 h of 25 mmol/L glucose, and after 6 h of exposure to 25 mmol/L in the presence of

after 1, 2, 3, 4, 5, and 6 h of exposure to 25 mmol/L, HAECs were collected, and cell lysates were immunoprecipitated with an antibody against VDAC. Phosphorylation of VDAC was evaluated using a p-Thr antibody. High-glucose treatment induced a significant increase in VDAC phosphorylation starting at 3 h (Fig. 2*C*). Increased VDAC threonine phosphorylation reached a maximum at 6 h (Fig. 2*C*). Consistent with the persistence of a decreased HK-II/VDAC association in 5 mmol/L glucose after transient exposure to 25 mmol/L glucose, VDAC phosphorylation induced by 6 h of exposure to 25 mmol/L glucose also persisted for 2 days of subsequent exposure to 5 mmol/L glucose (Fig. 2*C*, red bar). To demonstrate that the increased VDAC phosphorylation and subsequent dissociation of HK-II was mediated by GSK-3β, a cell-permeable peptide inhibitor of the kinase was used. Pretreatment with this inhibitor prevented both the high glucose–induced increase in VDAC threonine phosphorylation and the resulting HK-II/VDAC dissociation (Fig. 2*B* and *C*).

Transient Exposure to High Glucose Induces a Persistent Increase in GSK-3β Activity

Because these data suggest that high glucose increases GSK-3β activity, causing increased VDAC phosphorylation and consequent HK-II/VDAC dissociation, GSK3β activity was assessed directly by ^{32}P incorporation into a specific GSK-3β substrate in HAECs treated for 1, 2, 3, 4, 5, and 6 h with 25 mmol/L glucose (Fig. 2*D*). High glucose induced a significant increase in GSK-3β activity starting at 3 h, which reached a maximum at 6 h. These data mirror the time course of the increase in VDAC threonine phosphorylation induced by high glucose. Consistent with the persistence of increased VDAC threonine phosphorylation in 5 mmol/L glucose after transient exposure to 25 mmol/L glucose, increased GSK-3β activity induced by 6 h of exposure to 25 mmol/L glucose also persisted for 2 days of subsequent exposure to 5 mmol/L glucose (Fig. 2*D*, red bar).

Transient Exposure to High Glucose Induces a Persistent Decrease in Akt1 Activity

GSK-3β activity is controlled by the phosphorylation of specific residues by other kinases and is inhibited by phosphorylation at serine 9 by Akt, ILK, PKA, p90RSK, and PKC (9,10,22). Because increased GSK-3β activity induced by high glucose was prevented by overexpression of Akt-1CA (Fig. 2*D*), Akt1 activity was determined in HAECs exposed to high glucose. Cells were exposed to 25 mmol/L glucose, and Akt1 activity was measured 1, 2, 3, 4, 5, and 6 h after treatment. High glucose induced a significant decrease in Akt1 activity starting at 3 h, with activity reduced by 60% at 6 h (Fig. 2*E*). Consistent with the persistence of increased GSK-3β activity in 5 mmol/L glucose after transient exposure to 25 mmol/L glucose, decreased Akt1 activity induced by 6 h of exposure to 25 mmol/L glucose also persisted for 2 days of subsequent exposure to 5 mmol/L glucose (Fig. 2*E*, red bar).

Akt1 is activated by phosphoinositide 3-kinase–dependent phosphorylation at Ser473 and Thr308. Akt1 can be inactivated by several protein phosphatases, including PP2A, the lipid protein phosphatase PTEN, and PHLPP2 (23,24). Treatment with either of two PP2A-specific inhibitors, microcystin and okadaic acid, completely prevented the high glucose–induced decrease in Akt1 activity, suggesting that high glucose increases the activity of this phosphatase (Fig. 2*E*).

Transient Exposure to High Glucose Induces a Persistent Increase in PP2A Activity

Because PP2A inhibition prevented the decrease in Akt1 activity induced by high glucose, PP2A activity was then measured in HAECs treated for 1, 2, 3, 4, 5, and 6 h with 25 mmol/L glucose (Fig. 2*F*). High-glucose treatment induced a significant increase in PP2A activity by 2 h (2.7-fold) and reached a sixfold increase of control activity at 6 h (Fig. 2*F*). Consistent with the persistence of reduced Akt1 activity in 5 mmol/L glucose after transient exposure to 25 mmol/L glucose, increased PP2A activity induced by 6 h of exposure to 25 mmol/L glucose also persisted for 2 days of subsequent exposure to 5 mmol/L glucose (Fig. 2*F*, red bar). Overexpression of Mn-SOD prevented high glucose–induced PP2A activation (Fig. 2*F*), demonstrating that increased mitochondrial superoxide production was necessary for PP2A activation by high glucose. Overexpression of catalase

a peptide inhibitor of GSK-3β. Top panel shows IP-WB of VDAC:VDAC and VDAC:P-Thr. Bottom panel shows quantitation of IP-WB data from top panel. *D*: GSK-3β activity after transient exposure of HAECs to high glucose, after 2 days of 5 mmol/L glucose following 6 h of 25 mmol/L glucose, and after 6 h of exposure to 25 mmol/L in the presence of adenoviral (Ad) Akt-1CA. Activity was measured by ^{32}P incorporation into a GSK-3β–specific substrate. *E*: Akt1 activity after transient exposure of HAECs to high glucose, after 2 days of 5 mmol/L glucose following 6 h of 25 mmol/L glucose, and after 6 h of exposure to 25 mmol/L in the presence of PP2A inhibitors. *F*: PP2A activity after transient exposure of HAECs to high glucose, after 2 days of 5 mmol/L glucose following 6 h of 25 mmol/L glucose, and after 6 h of exposure to 25 mmol/L in the presence of Ad-Mn-SOD, Ad-catalase, or deferoxamine. *G*: Free iron concentration after transient exposure of HAECs to high glucose, after 2 days of 5 mmol/L glucose following 6 h of 25 mmol/L glucose, and after 6 h of exposure to 25 mmol/L in the presence of Ad-Mn-SOD. Free iron in HAECs was measured by EPR. *H*: Effect of Akt-DN or GSK-3β-CA on inner mitochondrial transmembrane potential and ROS level in HAECs in 5 mmol/L glucose. HAECs were exposed to 5 mmol/L glucose for 6 h after infection with Ad vectors expressing Akt-DN, GSK-3β-CA, or vector alone. Top panel shows representative photomicrographs of increased JC-1 red fluorescence, indicating increased mitochondrial membrane potential. Bottom panel shows ROS production measured by CM-H_2DCFDA. ROS data are mean ± SEM from three independent experiments with at least eight technical replicates. All other data are mean ± SD from five independent experiments. *$P < 0.05$. AU, arbitrary unit; d, days; DFO, deferoxamine; dpm, disintegrations per minute; inh, inhibitor; OD, optical density.

also prevented high glucose–induced PP2A activation, indicating that extramitochondrial diffusion of H_2O_2 produced by Mn-SOD was also necessary for PP2A activation. Finally, deferoxamine, an iron chelator, also prevented activation of PP2A by high glucose. Together, these results are consistent with PP2A activation by hydroxyl radicals generated by the reaction of H_2O_2 with free iron released from intramitochondrial stores by superoxide (25).

Transient Exposure to High Glucose Induces a Persistent Increase in Intracellular Free Iron

Mitochondrial superoxide production has been shown to cause increased free iron by inducing release of the metal from ferritin (26,27) and from mitochondrial iron-sulfur cluster proteins (28,29). To determine whether high glucose–induced mitochondrial superoxide production causes an increased release of free iron, cellular levels of the metal were measured by EPR. Free intracellular iron was measured in HAECs after 1, 2, 3, 4, 5, and 6 h of treatment with 25 mmol/L glucose. High glucose induced a significant increase in free iron levels after 2 h, reaching 2.8-fold after 6 h (Fig. 2*G*). Consistent with the persistence of increased PP2A activity in 5 mmol/L glucose after transient exposure to 25 mmol/L glucose, increased intracellular free iron levels induced by 6 h exposure to 25 mmol/L glucose also persisted for 2 days of subsequent exposure to 5 mmol/L glucose (Fig. 2*G*, red bar). Overexpression of Mn-SOD completely prevented high glucose–induced release of free iron, demonstrating that hyperglycemia-induced increase in mitochondrial superoxide production causes release of Fe^{2+} from intramitochondrial stores.

Mimicking Effects of High Glucose on Different Loop Components Increases $\Delta\Psi$ and ROS in Cells Exposed Only to 5 mmol/L Glucose

Detachment of VDAC-bound HK-II in cells incubated in 5 mmol/L glucose increases $\Delta\Psi$ and ROS production to the same level as does incubation in 25 mmol/L glucose (Fig. 2*A*). To demonstrate that altering other loop components has the same effect in cells exposed only to 5 mmol/L glucose, HAECs were cultured in 5 mmol/L glucose after infection with adenoviral vectors expressing either Akt-DN to mimic the effect of high glucose on Akt1 activity or a constitutively active form of GSK-3β (GSK-3β-CA) to mimic the effect of high glucose on GSK-3β. Overexpression of either Akt-DN or GSK-3β-CA induced an increase in $\Delta\Psi$ and ROS production to the same level as did incubation in 25 mmol/L glucose (Fig. 2*H*). A schematic representation of the multicomponent feedback loop that maintains persistent mitochondrial ROS production after transient exposure to high glucose is shown in Fig. 3.

Disruption of the Multicomponent Feedback Loop Reverses the Persistent Left Shift of the Glucose-ROS Dose-Response Curve Induced by Transient Exposure to High Glucose

To demonstrate that persistent activation of the multicomponent feedback loop stably shifts the glucose-ROS dose-response curve to the left, thus maintaining persistently increased mitochondrial ROS in 5 mmol/L glucose for days after transient exposure to high glucose, cells were incubated for 6 h in either 5 or 25 mmol/L glucose. Both groups of cells were then incubated in 5 mmol/L glucose for 2 days. After that 2-day incubation in 5 mmol/L glucose, cells transiently exposed to 25 mmol/L glucose at the beginning of the experiment had activity of the penultimate loop component GSK-3β normalized for 6 h using a degradable peptide inhibitor of GSK-3β (Fig. 4*A*, orange curve). This curve is shown in comparison with the curve from cells exposed to 5 mmol/L initially (Fig. 4*A*, blue curve) and the curve from cells initially exposed to 25 mmol/L glucose (Fig. 4*A*, red curve from Fig. 1).

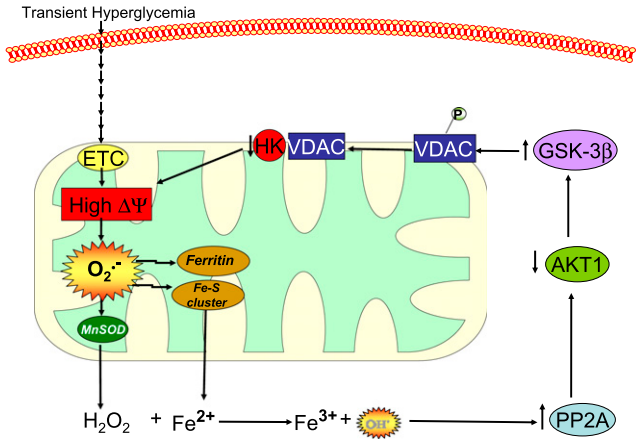

Figure 3—Schematic representation of the multicomponent feedback loop that maintains persistently increased ROS production after transient exposure to high glucose. Transient exposure to high glucose induces a transient increase in ETC flux, increasing $\Delta\Psi$ and thereby increasing mitochondrial superoxide production. In the mitochondria, this superoxide causes the release of Fe^{2+} from ferritin and iron sulfur cluster–containing proteins. This released free iron reacts with diffused superoxide-derived hydrogen peroxide to form hydroxyl radicals, which increase PP2A activity. Activated PP2A then dephosphorylates Akt1, decreasing its activity. Decreased Akt1 activity increases GSK-3β activity, which then increases VDAC threonine phosphorylation (P). Increased VDAC threonine phosphorylation decreases HK-II association with VDAC, which increases the $\Delta\Psi$ at physiologic levels of glucose. Operation of this loop causes a stable left shift of the glucose concentration-ROS dose-response curve, thereby maintaining increased ROS levels at normal glucose levels for days after transient exposure of cells to high glucose.

Brief Exposure to 12 mmol/L Glucose Has the Same Effects on Feedback Loop Components as Transient Exposure to a Higher Glucose Concentration, and GLP-1(9–36)^{amide} Prevents This

Because the data in Fig. 1*D* demonstrate that maximum ROS production in HAECs occurs at a glucose concentration of 12 mmol/L with no further increase at higher glucose concentrations, we next used 12 mmol/L glucose, a concentration often seen in hyperglycemic spikes in patients with type 1 diabetes, to show that brief exposure to this glucose concentration has the same effects on

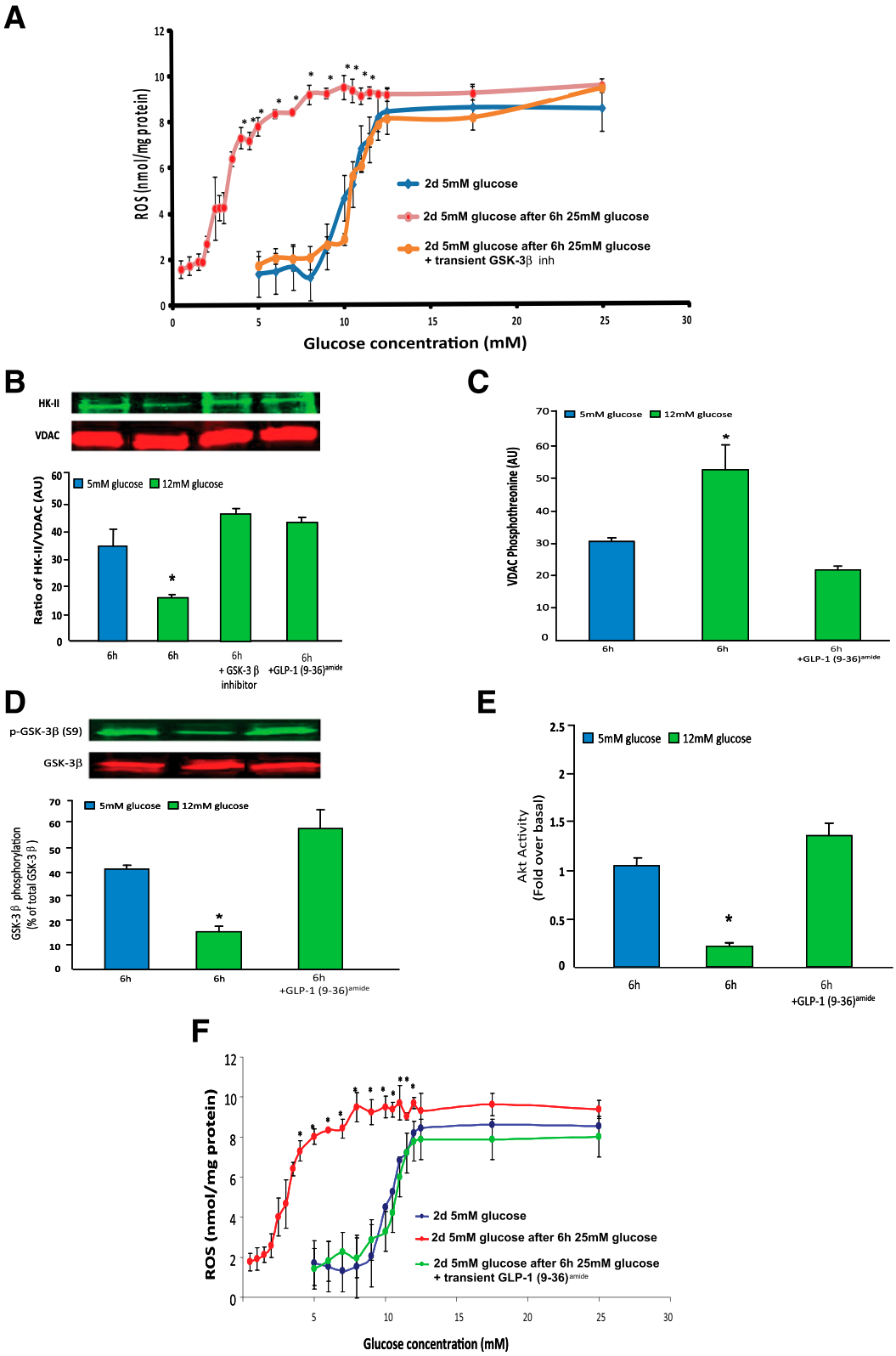

Figure 4—GLP-1(9–36)^{amide} reverses the persistent left shift of the glucose concentration-ROS dose-response curve caused by transient hyperglycemia. *A*: Glucose concentration-ROS dose-response curves. Glucose concentration-ROS dose-response curves from HAECs exposed to 25 mmol/L for 6 h followed by 2 days of 5 mmol/L glucose and then transiently treated with a peptide GSK-3β inhibitor (orange curve). This curve is shown in comparison with the glucose concentration-ROS curves from cells exposed to 5 mmol/L glucose for 2 days (blue curve) and the curve from cells exposed to 6 h of 25 mmol/L glucose followed by 5 mmol/L glucose for 2 days (red curve) from Fig. 1*D*. ROS levels were measured by CM-H_2DCFDA. ROS data are mean ± SEM from three independent experiments with at least eight technical replicates. *$P < 0.05$. *B–E*: Effect of GLP-1(9–36)^{amide} on feedback loop components. HAECs were exposed to 25 mmol/L glucose for 6 h

feedback loop components as brief exposure to a higher glucose concentration. We also determined the effect of the GLP-1 cleavage product GLP-1(9–36)^{amide}, which is rapidly produced in vivo by dipeptidyl peptidase IV cleavage, on components of the ROS-generating feedback loop.

HAECs were exposed to 12 mmol/L glucose for 6 h in the presence or absence of GLP-1(9–36)^{amide} or a GSK-3β inhibitor peptide and HK-II/VDAC association was evaluated by IP-WB. GLP-1(9–36)^{amide} prevented the high glucose–induced decrease in HK-II/VDAC association as effectively as the GSK-3β inhibitor peptide (Fig. 4*B*). GLP-1(9–36)^{amide} also prevented the high glucose–induced increase in VDAC phosphorylation (Fig. 4*C*), GSK-3β activity measured as p-GSK-3β (S9)/GSK-3β was increased to the same extent by 12 mmol/L glucose as it was by higher glucose concentrations. GLP-1(9–36)^{amide} completely prevented this (Fig. 4*D*). Moreover, Akt activity was reduced to the same extent by 6 h of exposure to 12 mmol/L glucose as it was by higher glucose concentrations, and GLP-1(9–36)^{amide} completely prevented this (Fig. 4*E*).

Feedback Loop Disruption by the GLP-1 Cleavage Product GLP-1(9–36)^{amide} Reverses the Persistent Left Shift of the Glucose Concentration-ROS Dose-Response Curve After Transient Hyperglycemia, Thereby Normalizing Persistent ROS Production and Its Pathophysiologic Consequences in Cultured Endothelial Cells and in Mice

To demonstrate that GLP-1(9–36)^{amide} reverses the left shift of the glucose-ROS dose-response curve, HAECs previously exposed for 6 h to 25 mmol/L glucose followed by 5 mmol/L glucose for 2 days were transiently exposed to the peptide on day 2, and a glucose concentration-ROS dose-response experiment was performed. Transient exposure to GLP-1(9–36)^{amide} completely reversed the persistent left-shifted glucose concentration-ROS dose-response curve (Fig. 4*F*, green curve). The glucose concentration-ROS dose-response obtained is superimposed on the curve from cells exposed to 5 mmol/L glucose for 2 days (blue curve) and from cells exposed to 6 h of 25 mmol/L glucose followed by 5 mmol/L glucose for 2 days (red curve) from Fig. 1. The effect of GLP-1(9–36)^{amide} and its precursor peptide GLP-1(7–36)^{amide} on ROS generation after transient exposure to 25 mmol/L glucose is shown in Supplementary Fig. 3.

ROS induced by high glucose directly inhibit the activity of the endothelial cell enzyme PGI_2 (30). In experimental diabetes, this has been shown to accelerate both nephropathy and cardiac fibroblast proliferation (31–33).

In cultured HAECs, prostacyclin activity was reduced 80% after 2 days' incubation in 5 mmol/L glucose after prior transient exposure to 25 mmol/L glucose (data not shown). To demonstrate that transient hyperglycemia also induces persistent ROS production and consequent PGI_2 inhibition in vivo, we measured PGI_2 activity in a transient hyperglycemia mouse model (18). In nondiabetic mice, PGI_2 activity was measured in mouse aortas 6 days after transient hyperglycemia, and despite normal glucose metabolism for 6 days, PGI_2 activity was still reduced >90% (Fig. 5, bar 2). Because the half-life of PGI_2 is 2.5 h (34), the persistent inhibition of its activity for 6 days in normoglycemic, nondiabetic mice after transient hyperglycemia is consistent with continuous production of ROS maintained by the multicomponent feedback loop. To test this hypothesis, continuous ROS production was blocked by transient treatment with GLP-1(9–36)^{amide}. Two days after transient hyperglycemia, a micro-osmotic pump containing GLP-1(9–36)^{amide} (300 μg/mL) was inserted in the mice for 24 h and then removed (Fig. 5, top panel). As shown in Fig. 5, bar 3, 3 days after the GLP-1(9–36)^{amide} was removed, the dramatic reduction of PGI_2 activity, which persisted for 6 days in nondiabetic animals after transient hyperglycemia (Fig. 5, bar 2), was completely normalized. Because in mouse liver the half-life of GLP-1(9–36)^{amide} is 52 min and that of its potentially bioactive cleavage product GLP-1(28–36)^{amide} is 13 min (35), the persistent effect on PGI_2 activity is most consistent with disruption of the ROS-generating feedback loop established by transient hyperglycemia.

DISCUSSION

In this study, we show that 4–6 h of exposure to a level of high glucose frequently seen in the glycemic spikes of patients with type 1 diabetes activates a multicomponent feedback loop that causes a stable left shift of the glucose concentration-ROS dose-response curve. This left shift causes persistent mitochondrial overproduction of ROS for days after glucose concentration is normalized. In HAECs, the GLP-1 cleavage product GLP-1(9–36)^{amide} reversed the persistent left shift caused by transient hyperglycemia. Similarly, in nondiabetic mice, brief disruption of the feedback loop with GLP-1(9–36)^{amide} 2 days after transient hyperglycemia normalized persistent ROS inactivation of endothelial cell PGI_2, a defect believed to play an important role in the pathogenesis of both diabetic nephropathy and cardiac fibrosis (30–32).

with or without 100 pmol/L GLP-1(9–36)^{amide}. Cells exposed to 5 mmol/L glucose were used as controls (blue bars). *B*: HK-II/VDAC association. A peptide inhibitor of GSK-3β was used as control. *C*: VDAC phosphorylation: quantitation of IP-WB data. *D*: GSK-3β phosphorylation. Top panel shows IP-WB of GSK-3β:GSK-3β and GSK-3β:p-GSK-3β (S9). Bottom panel shows quantitation of IP-WB data from top panel. *E*: Akt1 activity. Data are mean ± SD from five independent experiments. *$P < 0.01$. *F*: Effect of GLP-1(9–36)^{amide} on glucose concentration-ROS dose-response curves. Glucose concentration-ROS dose-response curve from HAECs exposed to 25 mmol/L for 6 h followed by 2 days of 5 mmol/L glucose and then transiently treated with GLP-1(9–36)^{amide} (green curve). This curve has been superimposed on the glucose concentration-ROS curves from *A*. ROS levels were measured by CM-H_2DCFDA. ROS data are mean ± SEM from three independent experiments with at least eight technical replicates. *$P < 0.05$. AU, arbitrary unit; d, days; inh, inhibitor.

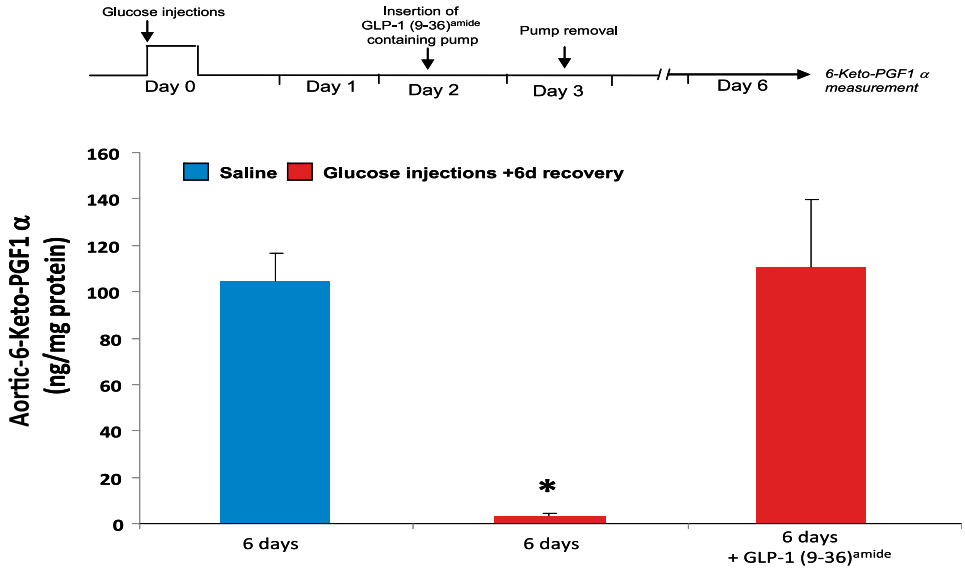

Figure 5—GLP-1(9–36)^{amide} reverses the persistent reduction of PGI_2 caused by transient hyperglycemia in vivo. Top panel shows experiment schematic. Bottom panel shows findings in C57BL/6 mice (n = 5/group) that received four sequential injections of glucose 3 g/kg i.p. (red bars) or an equivalent volume of 0.9% saline (blue bar) at 2-h intervals. Two days after transient hyperglycemia, a micro-osmotic pump containing GLP-1(9–36)^{amide} (300 μg/mL) was inserted in the mice for 24 h and then removed. Aortas were removed and PGI_2 activity measured in all groups 6 days after initial glucose or saline injections. Data are mean ± SD. *P < 0.01. d, days.

Because hyperglycemia-induced overproduction of mitochondrial ROS also initiates many of the other complex series of molecular events that result in diabetic tissue damage (36), these data suggest that hyperglycemic spikes high enough to activate persistent ROS production during subsequent periods of normal glycemia but too brief to affect the HbA_{1c} value are a major determinant of the 89% of diabetes complications risk not captured by HbA_{1c} (3). The stable left shift of the glucose concentration-ROS dose-response curve induced by short exposure to high glucose is an example of bistability, a fundamental property of many biological systems in which the system can be in either of two alternative, stable steady states (37,38). Bistability is based on the continued activation or inhibition of feedback loops. For example, transient exposure of *Xenopus* oocytes to progesterone induces stable cellular differentiation, which persists in the absence of progesterone (37). Similarly, both stable transformation of differentiated cells into induced pluripotent stem cells and stable transformation of embryonic stem cells into differentiated cells involve stable feedback loops initiated by transient exposure to a small number of transcription factors (39,40).

In this study, 1 h of transient exposure to high glucose maximally increased ROS in HAECs. However, 4–6 h of exposure to high glucose were required for the persistent generation of ROS after normoglycemia restoration. These data suggest that a critical change in other loop components takes at least 4 h to establish. It may also reflect the time course of other ROS-mediated effects.

Why does increased ROS not activate a negative feedback loop to restore homeostasis as proposed by Brand and colleagues (41)? A plausible answer is suggested by the work of Harper and colleagues (42,43) who confirmed that uncoupling proteins (UCPs) 2 and 3 are activated by ROS and discovered that reversible posttranslational modification of UCPs with glutathione reverses ROS-mediated activation of UCPs. Because mitochondrial ROS can trigger both protein glutathionylation and protein deglutathionylation through the enzyme glutaredoxin 2, 4–6 h of sufficiently high levels of ROS in the presence of high glucose may adversely affect *S*-glutathionylation of UCPs and a number of other mitochondrial proteins (42).

In the current study, GLP-1(9–36)^{amide} was shown to prevent the excess VDAC phosphorylation induced by transient hyperglycemia, the excess activation of GSK-3β responsible for this, and the decreased association of HK-II with VDAC and to prevent the inhibition of Akt activity caused by transient hyperglycemia. As a result, GLP-1(9–36)^{amide} reversed the persistent left shift of the glucose concentration-ROS dose-response curve caused by transient hyperglycemia and thereby reversed the ROS-dependent inactivation of PGI_2. GLP-1(9–36)^{amide} is the cleavage product of the incretin hormone GLP-1(7–36)^{amide}. Studies have shown that GLP-1(9–36)^{amide}, initially considered to be an inactive degradation product of GLP-1, performs important physiologic functions distinct from its precursor (12). GLP-1(9–36)^{amide} has been reported to have unique extrapancreatic insulin-like actions in the heart, vasculature, and liver, which appear not to be mediated through the GLP-1 receptor (35). In HAECs, GLP-1(9–36)^{amide} activate cardioprotective signaling pathways, whereas GLP-1 receptor agonists do not (44). Whether the effects of GLP-1(9–36)^{amide} in the current study are mediated through an unidentified cell surface receptor or through

further degradation to a nonapeptide possibly targeted to mitochondria remains to be elucidated.

Paneni et al. (45) proposed an ROS-generating feedback loop in HAECs consisting of two components: p66Shc and protein kinase C (PKC) βII. They reported that continuous exposure of endothelial cells to 25 mmol/L glucose increased expression of the adaptor protein p66Shc and activated p66Shc by a PKC βII–dependent mechanism. In contrast, in the current experiments, we did not observe any change in either p66Shc protein levels or increased p66Shc phosphorylation (data not shown). Our observations that GLP-1(9–36)^{amide} prevents the high glucose–induced changes in feedback loop components identified in this study and that this peptide reverses persistent ROS inactivation of PGI_2 after transient hyperglycemia in nondiabetic mice support the feedback loop elucidated here.

Hyperglycemia-induced overproduction of mitochondrial ROS initiates many of the complex series of molecular events that result in diabetic tissue damage (36), and transgenic expression of the antioxidant enzyme SOD prevents each complication in experimental diabetes (46–48). We have previously observed (49) that in endothelial Rho-zero (cells that have been depleted of their own mitochondrial DNA by prolonged incubation with ethidium bromide and consequently lacking functional mitochondria), exposure to high glucose failed to increase ROS production (50). Thus, it appears that the mitochondria are required for the initiation of hyperglycemia-induced superoxide production. Published evidence has indicated that this in turn can activate a number of other superoxide production pathways that may amplify the original damaging effect of hyperglycemia, including activation of NADPH oxidases and uncoupling of endothelial nitric oxide synthase (6).

Because the major cause of death in people with type 1 diabetes is cardiovascular disease (CVD), HAECs were used in the current study. During the DCCT, the small number of CVD events in the relatively young cohort precluded a determination of the effect of HbA_{1c} on the risk of CVD. However, the DCCT data show that at least 89% of variation in risk of diabetic retinopathy and a similar percentage of risk of microalbuminuria or albuminuria are not captured by mean HbA_{1c} values (2,3). In 2005, long-term follow-up data on the DCCT/EDIC cohort showed no difference in mean HbA_{1c} values between the two EDIC study groups. However, the hazard ratio for risk of nonfatal myocardial infarction, stroke, or death from CVD was increased 2.5- to 2.9-fold in patients with either microalbuminuria or albuminuria (51).

The data presented here suggest that the 89% of variation in risk of diabetic microalbuminuria or albuminuria not captured by mean HbA_{1c} values in the DCCT cohort may reflect transient above-threshold spikes of hyperglycemia that continue to activate damaging mechanisms for days of subsequent near-normal glycemia. The phenomenon and mechanism described in this study provide a basis for the development of new biomarkers to complement HbA_{1c} and novel therapeutic agents, including GLP-1(9–36)^{amide}, for the prevention and treatment of diabetes complications.

Acknowledgments. The authors thank Aviv Bergman, Chair, Department of Systems and Computational Biology, Albert Einstein College of Medicine, for helpful discussions during the course of this work. The authors also thank Morris Birnbaum, Willard and Rhoda Ware Professor of Diabetes and Metabolic Diseases, University of Pennsylvania, for providing plasmids, adenoviral vectors, and advice.

Funding. F.G. was supported by a European Diabetes Foundation/Lilly postdoctoral fellowship. X.D. was supported in part by National Institutes of Health (NIH) grant 5P60-DK-020541. A.C. was supported by an Italian Ministry of University and Scientific Research (MIUR) fellowship. G.J.G. was supported by National Science Foundation grant CHE-1335708. M.D. and I.G. were supported by MIUR grant Progetti di ricerca di interesse nazionale 08:20082P8CCE_002. A.R. was supported by "Progetti di Ateneo of Padua University." A.N.M. was supported by NIH grant P01-DK-054441. This project was funded by NIH grant 1R01-DK-33861, JDRF grants 8-2003-784 and 4-2004-804, and JDRF Scholar Award 16-2006-501 (to M.B.).

Duality of Interest. A.S.D. was supported by Seahorse Bioscience. No other potential conflicts of interest relevant to this article were reported.

Author Contributions. F.G. performed the experiments and contributed to the study concept, research design, and drafting of the manuscript. X.D. performed the experiments and contributed to the study concept and research design. A.C., G.J.G., and M.S.S. performed the experiments. M.D., I.G., A.S.D., and A.N.M. contributed to the discussion and data interpretation. A.R. and O.M. provided critical reagents and advice for the experiments. M.B. contributed to the study concept, research design, and drafting of the manuscript. M.B. is the guarantor of this work and, as such, had full access to all the data in the study and takes responsibility for the integrity of the data and the accuracy of the data analysis.

References

1. The Diabetes Control and Complications Trial Research Group. The effect of intensive treatment of diabetes on the development and progression of long-term complications in insulin-dependent diabetes mellitus. N Engl J Med 1993;329:977–986

2. The Diabetes Control and Complications Trial Research Group. The relationship of glycemic exposure (HbA_{1c}) to the risk of development and progression of retinopathy in the diabetes control and complications trial. Diabetes 1995;44:968–983

3. Lachin JM, Genuth S, Nathan DM, Zinman B, Rutledge BN; DCCT/EDIC Research Group. Effect of glycemic exposure on the risk of microvascular complications in the diabetes control and complications trial—revisited. Diabetes 2008;57:995–1001

4. Kovatchev BP, Otto E, Cox D, Gonder-Frederick L, Clarke W. Evaluation of a new measure of blood glucose variability in diabetes. Diabetes Care 2006;29:2433–2438

5. Brownlee M, Hirsch IB. Glycemic variability: a hemoglobin A1c-independent risk factor for diabetic complications. JAMA 2006;295:1707–1708

6. Giacco F, Brownlee M. Oxidative stress and diabetic complications. Circ Res 2010;107:1058–1070

7. Korshunov SS, Skulachev VP, Starkov AA. High protonic potential actuates a mechanism of production of reactive oxygen species in mitochondria. FEBS Lett 1997;416:15–18

8. Pastorino JG, Hoek JB. Regulation of hexokinase binding to VDAC. J Bioenerg Biomembr 2008;40:171–182

9. Medina M, Garrido JJ, Wandosell FG. Modulation of GSK-3 as a therapeutic strategy on tau pathologies. Front Mol Neurosci 2011;4:24

10. Medina M, Wandosell F. Deconstructing GSK-3: the fine regulation of its activity. Int J Alzheimers Dis 2011;2011:479249
11. Pastorino JG, Hoek JB, Shulga N. Activation of glycogen synthase kinase 3beta disrupts the binding of hexokinase II to mitochondria by phosphorylating voltage-dependent anion channel and potentiates chemotherapy-induced cytotoxicity. Cancer Res 2005;65:10545–10554
12. Tomas E, Stanojevic V, Habener JF. GLP-1-derived nonapeptide GLP-1(28-36)amide targets to mitochondria and suppresses glucose production and oxidative stress in isolated mouse hepatocytes. Regul Pept 2011;167:177–184
13. Ma T, Du X, Pick JE, Sui G, Brownlee M, Klann E. Glucagon-like peptide-1 cleavage product GLP-1(9-36) amide rescues synaptic plasticity and memory deficits in Alzheimer's disease model mice. J Neurosci 2012;32:13701–13708
14. Chiara F, Castellaro D, Marin O, et al. Hexokinase II detachment from mitochondria triggers apoptosis through the permeability transition pore independent of voltage-dependent anion channels. PloS One 2008;3:e1852
15. D'Apolito M, Du X, Zong H, et al. Urea-induced ROS generation causes insulin resistance in mice with chronic renal failure. J Clin Invest 2010;120:203–213
16. Nishikawa T, Edelstein D, Du XL, et al. Normalizing mitochondrial superoxide production blocks three pathways of hyperglycaemic damage. Nature 2000;404:787–790
17. Srinivasan C, Liba A, Imlay JA, Valentine JS, Gralla EB. Yeast lacking superoxide dismutase(s) show elevated levels of "free iron" as measured by whole cell electron paramagnetic resonance. J Biol Chem 2000;275:29187–29192
18. Okabe J, Orlowski C, Balcerczyk A, et al. Distinguishing hyperglycemic changes by Set7 in vascular endothelial cells. Circ Res 2012;110:1067–1076
19. Du X, Edelstein D, Obici S, Higham N, Zou MH, Brownlee M. Insulin resistance reduces arterial prostacyclin synthase and eNOS activities by increasing endothelial fatty acid oxidation. J Clin Invest 2006;116:1071–1080
20. Murphy MP. How mitochondria produce reactive oxygen species. Biochem J 2009;417:1–13
21. Adam-Vizi V, Chinopoulos C. Bioenergetics and the formation of mitochondrial reactive oxygen species. Trends Pharmacol Sci 2006;27:639–645
22. Hardt SE, Sadoshima J. Glycogen synthase kinase-3beta: a novel regulator of cardiac hypertrophy and development. Circ Res 2002;90:1055–1063
23. Ugi S, Imamura T, Maegawa H, et al. Protein phosphatase 2A negatively regulates insulin's metabolic signaling pathway by inhibiting Akt (protein kinase B) activity in 3T3-L1 adipocytes. Mol Cell Biol 2004;24:8778–8789
24. Liao Y, Hung MC. Physiological regulation of Akt activity and stability. Am J Transl Res 2010;2:19–42
25. Horowitz MP, Greenamyre JT. Mitochondrial iron metabolism and its role in neurodegeneration. J Alzheimers Dis 2010;20(Suppl. 2):S551–S568
26. Welch KD, Davis TZ, Van Eden ME, Aust SD. Deleterious iron-mediated oxidation of biomolecules. Free Radic Biol Med 2002;32:577–583
27. Williams DM, Lee GR, Cartwright GE. The role of superoxide anion radical in the reduction of ferritin iron by xanthine oxidase. J Clin Invest 1974;53:665–667
28. Kell DB. Iron behaving badly: inappropriate iron chelation as a major contributor to the aetiology of vascular and other progressive inflammatory and degenerative diseases. BMC Med Genomics 2009;2:2
29. Cantu D, Schaack J, Patel M. Oxidative inactivation of mitochondrial aconitase results in iron and H2O2-mediated neurotoxicity in rat primary mesencephalic cultures. PLoS One 2009;4:e7095
30. Zou MH. Peroxynitrite and protein tyrosine nitration of prostacyclin synthase. Prostaglandins Other Lipid Mediat 2007;82:119–127
31. Zhao HJ, Wang S, Cheng H, et al. Endothelial nitric oxide synthase deficiency produces accelerated nephropathy in diabetic mice. J Am Soc Nephrol 2006;17:2664–2669
32. Nasu T, Kinomura M, Tanabe K, et al. Sustained-release prostacyclin analog ONO-1301 ameliorates tubulointerstitial alterations in a mouse obstructive nephropathy model. Am J Physiol Renal Physiol 2012;302:F1616–F1629
33. Chen Y, Yang S, Yao W, et al. Prostacyclin analogue beraprost inhibits cardiac fibroblast proliferation depending on prostacyclin receptor activation through a TGF β-Smad signal pathway. PLoS One 2014;9:e98483
34. Nusing R, Goerig M, Habenicht AJ, Ullrich V. Selective eicosanoid formation during HL-60 macrophage differentiation. Regulation of thromboxane synthase. Eur J Biochem 1993;212:371–376
35. Sharma R, McDonald TS, Eng H, et al. In vitro metabolism of the glucagon-like peptide-1 (GLP-1)-derived metabolites GLP-1(9-36)amide and GLP-1(28-36)amide in mouse and human hepatocytes. Drug Metab Dispos 2013;41:2148–2157
36. Brownlee M. Biochemistry and molecular cell biology of diabetic complications. Nature 2001;414:813–820
37. Xiong W, Ferrell JE Jr. A positive-feedback-based bistable 'memory module' that governs a cell fate decision. Nature 2003;426:460–465
38. Burrill DR, Silver PA. Making cellular memories. Cell 2010;140:13–18
39. Macarthur BD, Ma'ayan A, Lemischka IR. Systems biology of stem cell fate and cellular reprogramming. Nat Rev Mol Cell Biol 2009;10:672–681
40. Takahashi K, Tanabe K, Ohnuki M, et al. Induction of pluripotent stem cells from adult human fibroblasts by defined factors. Cell 2007;131:861–872
41. Echtay KS, Roussel D, St-Pierre J, et al. Superoxide activates mitochondrial uncoupling proteins. Nature 2002;415:96–99
42. Mailloux RJ, McBride SL, Harper ME. Unearthing the secrets of mitochondrial ROS and glutathione in bioenergetics. Trends Biochem Sci 2013;38:592–602
43. Mailloux RJ, Seifert EL, Bouillaud F, Aguer C, Collins S, Harper ME. Glutathionylation acts as a control switch for uncoupling proteins UCP2 and UCP3. J Biol Chem 2011;286:21865–21875
44. Ban K, Kim KH, Cho CK, et al. Glucagon-like peptide (GLP)-1(9-36)amide-mediated cytoprotection is blocked by exendin(9-39) yet does not require the known GLP-1 receptor. Endocrinology 2010;151:1520–1531
45. Paneni F, Mocharla P, Akhmedov A, et al. Gene silencing of the mitochondrial adaptor p66(Shc) suppresses vascular hyperglycemic memory in diabetes. Circ Res 2012;111:278–289
46. Shen X, Zheng S, Metreveli NS, Epstein PN. Protection of cardiac mitochondria by overexpression of MnSOD reduces diabetic cardiomyopathy. Diabetes 2006;55:798–805
47. Vincent AM, Russell JW, Sullivan KA, et al. SOD2 protects neurons from injury in cell culture and animal models of diabetic neuropathy. Exp Neurol 2007;208:216–227
48. Kowluru RA, Kowluru V, Xiong Y, Ho YS. Overexpression of mitochondrial superoxide dismutase in mice protects the retina from diabetes-induced oxidative stress. Free Radic Biol Med 2006;41:1191–1196
49. Brownlee M. The pathobiology of diabetic complications: a unifying mechanism. Diabetes 2005;54:1615–1625
50. King MP, Attardi G. Isolation of human cell lines lacking mitochondrial DNA. Methods Enzymol 1996;264:304–313
51. Nathan DM, Cleary PA, Backlund JY, et al.; Diabetes Control and Complications Trial/Epidemiology of Diabetes Interventions and Complications (DCCT/EDIC) Study Research Group. Intensive diabetes treatment and cardiovascular disease in patients with type 1 diabetes. N Engl J Med 2005;353:2643–2653